Reaction
Chemistry &
Engineering

PAPER

View Article Online
View Journal

Check for updates

Cite this: DOI: 10.1039/d2re00053a

Synergistic hydrothermal treatment of food waste digestate residues and incineration fly ash: dehydration performance and heavy metals safety†

Yu Wang,[ab] Guangwei Yu,*[ac] Jiajia Lin,[ab] Ruqing Jiang,[ab] Xinhai Xu,[ab] Shengyu Xie[d] and Yin Wang[a]

Received 15th February 2022,
Accepted 23rd April 2022

DOI: 10.1039/d2re00053a

rsc.li/reaction-engineering

The poor dewaterability of digestate residues (DRs) and the toxicity of fly ash (FA) limit their processing and utilization at the recycling stage. Hydrothermal treatment is a promising technology for deep dehydration and detoxification of waste. In the present study, synergistic hydrothermal treatment (HTT) of DRs and FA was conducted to investigate the dehydration performance and heavy metals (HMs) safety. The results showed that 10 wt% FA maximized the dehydration performance of DRs and promoted the conversion of loosely bound extracellular polymeric substances (EPS) and tightly bound EPS to soluble EPS (S-EPS) which facilitated the removal of sticky S-EPS, resulting in a reduction in the normalized capillary suction time to 0.358 s L g^{-1} and an increase in solids content to 36.61 g per 100 g. Moreover, HTT promoted the conversion of HM fractions in solid products from bioavailable fractions to stable fractions and the potential ecological risks of solids were low. This study provided a cost-effective, efficient and safe process for co-treating DRs and FA with high application prospects.

1. Introduction

As the catering industry expands to meet the demands of the increasing social economy, the amount of food waste (FW) has increased dramatically. For example, the total amount of FW in China still increased to 125 billion kilograms despite the impact of the coronavirus in early 2020.[1] Anaerobic digestion (AD) has gradually become a popular method of FW disposal, accounting for about 70% of processing capacity because of its sustainability and reduced environmental impact.[2,3] Plenty of usable secondary energy can be made available by AD,[4] but it also produces large quantities of anaerobic digestate residues (DRs).[5] Meanwhile, only 15–40 wt% of organic matter is consumed for biogas production during the anaerobic fermentation of FW,[6] while the remaining liquid and solid digestate constituted secondary solid waste. Each year, 17.5 billion kilograms of DRs will be produced in China, calculated based on 200 kg DRs per ton of FW. In addition to their high water content and viscosity, DRs may contain hazardous substances, such as pathogens and heavy metals (HMs) which are difficult to be treated.[7] Hence, the inappropriate disposal of DRs may result in secondary groundwater and soil pollution, which is a threat to human health.[8] In China, the main disposal methods for DRs include fertilizer utilization,[9] sanitary landfills, incineration and aerobic composting.[10,11] Unfortunately, the high water content of DRs is the main challenge for their subsequent processing and utilization. DRs are heterogeneous amorphous materials that are extremely difficult to isolate from the water phase using mechanical separation methods. Therefore, to reduce the costs of transportation and handling, the most important part of DR treatment prior to disposal is the reduction of volume by dehydration separation.[12]

Currently, some dehydration techniques for organic waste, such as ultrasonic treatments,[13] microwave-acid pretreatments,[14] acid/alkali treatments,[15] photo-Fenton/Fenton oxidation technology and combinations of these processes,[16] have achieved good dehydration results. However, the high cost and low disposal capacity of these technologies limit their large-scale application. Deep-dehydration technology has been used in China, and chemical conditioning or other auxiliary sample treatments

---

[a] CAS Key Laboratory of Urban Pollutant Conversion, Institute of Urban Environment, Chinese Academy of Sciences, Xiamen 361021, Fujian, China. E-mail: gwyu@iue.ac.cn
[b] University of Chinese Academy of Sciences, Beijing 101408, China
[c] Fujian Municipal Solid Waste Resource Recovery Technology Research Center, Xiamen 361021, Fujian, China
[d] Graduate School of Environmental Studies, Tohoku University, 6-6-07 Aoba, Aramaki-aza, Aoba-ku, Sendai, Miyagi 980-8579, Japan

† Electronic supplementary information (ESI) available. See DOI: **https://doi.org/10.1039/d2re00053a**

such as filter press and centrifuge dehydration are necessary to improve the final dehydration effect.[17] At present, the usage of coagulants has gained more attention for enhancing the dehydration performance of solid waste. Alum, polyaluminum chloride, $FeCl_3$ and $FeSO_4$, as common inorganic coagulants, require large doses and careful pH control, which will increase the cost of the disposal process. Electro-osmosis-assisted sludge dehydration technology utilizes a low electric field to remove moisture and is usually combined with traditional dehydration technology to achieve a greater effect.[18] In practice, its cost-effectiveness is compromised by equipment corrosion and high energy consumption. Among the various treatment methods, hydrothermal treatment (HTT) exhibits many benefits due to the destruction of microorganisms at high temperatures and pressures.[19,20] In addition, HTT has high scale-up potential for industrial applications and good stabilization of HMs.[21] Some HTT studies showed that HTT improved the dehydration performance of DRs and the utilization of products.[22] The addition of alkaline substances such as $Ca(OH)_2$ during the HTT process can further improve the dehydration performance though this may increase the overall costs.[19]

Fly ash (FA), a type of solid waste from the incineration of municipal solid waste (MSW), has similarities to inorganic conditioners, *e.g.*, high alkalinity and high calcium content, which have been verified to be the important factors in the destruction of extracellular polymers.[23] The incineration of MSW produces 6–7 million tons of FA every year in China, which is equivalent to 30–50 kg per ton of MSW.[24] Recently, HTT, biodegradation, plasma, mechanochemistry, photocatalytic techniques and so on all show excellent detoxification effects, which are beneficial to the application of FA as a resource.[25] Among them, HTT has been developed into a promising technology for FA harmless treatment considering HM stabilization, dechlorination, and dioxin degradation, in addition to the advantages of large capacity, the high degradation rate of organic pollutants, and commercial application potential.[26,27] Based on the above advantages, the synergistic hydrothermal treatment of DRs and FA can simultaneously achieve dehydration of DRs and detoxification of FA in the same equipment or process. Furthermore, the minerals in FA can catalytically enhance the production of valuable chemicals and fuel from further pyrolysis after HTT.[23] Therefore, synergistic hydrothermal treatment of DRs and FA might have considerable mutual advantages associated with their safer disposal and better utilization. It is required to investigate the effects of FA addition on the dehydration mechanism of DRs during HTT and the safety of products because of limited reports.

In this study, the dehydration performance and product safety during the synergistic hydrothermal treatment of DRs and FA were investigated. A range of chemical, physical, and spectroscopic methods were used to investigate the mechanism of dehydration. HMs were determined in the four fractions obtained from the three-step extraction procedure of the European Community Bureau of Reference (BCR), and the toxicity characteristic leaching procedure (TCLP) and potential ecological risk indices (RIs) were used to evaluate exposure to HMs.

2. Materials and methods

2.1. Materials

DRs (moisture content 80.27 wt%) and FA were obtained from an anaerobic digestion treatment plant for FW (capacity of 3×10^5 kg d^{-1}) and an MSW incineration plant using grate furnace technology in Dongguan, China, respectively. DRs and FA were stored at 4 °C and in a desiccator, respectively, and their basic properties are shown in the ESI.†

2.2. HTT device and procedure

All treatments were carried out in an FCF-2L high-pressure reaction kettle (ZZKD Instrument Equipment, Zhengzhou City, China) equipped with a central electric stirring device which is shown in Fig. 1. The mixed samples of DRs and FA (1000 g), prepared in wet base weight ratios of 100 : 0, 95 : 5, 90 : 10 and 85 : 15, were evenly mixed with ultra-pure water (200 g) before adding to the kettle. The sealed kettle was heated from 30 °C to 180 °C at 10 °C min^{-1}, maintained for 30 minutes and then cooled to 30 °C. The obtained HTT samples (DFs) were labelled DF100, DF95, DF90 and DF85. The DFs and DRs were centrifuged, dried, ground and passed through a 100-mesh sieve. These treated hydrothermal samples (DFCs) and DRs were labelled DFC100, DFC95, DFC90, DFC85 and DRC. For comparison, 100% FA was subjected to HTT (FAH) and centrifugation/sieving/drying (FAHC).

2.3. Analytical methods

2.3.1 Dehydration performance index. Capillary suction time (CST, s) which is usually used to characterize dehydration performance, was measured using a CST unit (Paragon Technology, Hangzhou, China). To eliminate the influence of solids, normalized CST (NCST, s L g^{-1}) was obtained by dividing the CST value by the total suspended solids measured.[28] The solids content was obtained by centrifugation at 2000*g* for 10 minutes according to the American Public Health Association standard method.[29]

2.3.2 Characteristics of DRs, DFs, and DFCs. The particle size distributions of DRs and DFs were obtained using an MS200 submicron/micron (laser) particle size/particle number analyser (Malvern Panalytical, UK). Zeta potentials were measured with a Zeta PALS zeta potential analyzer (Brookhaven Instruments, NY, USA) and a nano/submicron particle size analyser (Malvern Panalytical, UK). A DV-C digital viscometer (Brookfield, China) was used to measure viscosity. The microstructures were measured by scanning electron microscopy (SEM, S-4800, Hitachi, Japan). The surface functional groups of DRC and DFCs were characterized using a Nicolet™ iS™ 10 Fourier transform

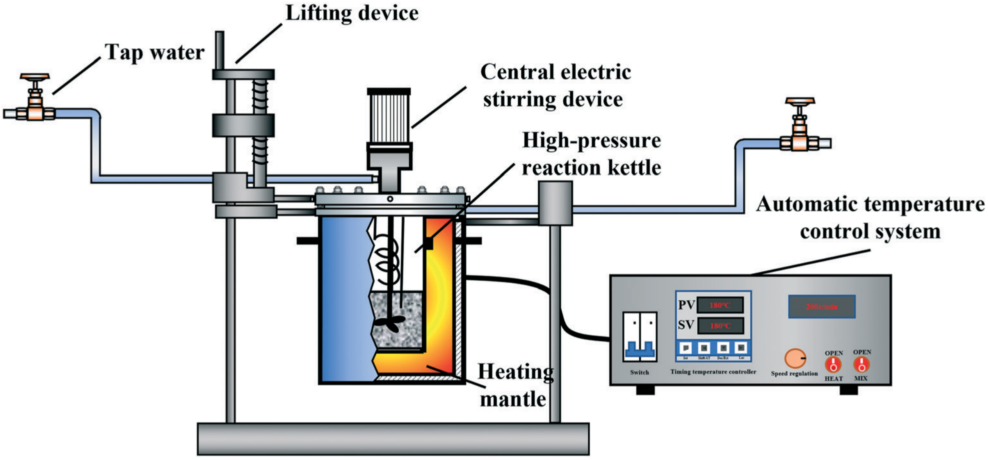

Fig. 1 Schematic diagram of the hydrothermal apparatus.

infrared (FTIR) spectrometer (ThermoFisher Scientific, USA). The analysis of mineral elements was determined using X-ray fluorescence spectrometry (XRF) on an Axios$^{\mathrm{mAX}}$ instrument (PANalytical, The Netherlands).

2.3.3 Extraction and analysis of extracellular polymeric substances (EPS). DRs or DFs (40 mL) were centrifuged at 3000*g* for 10 min, and the supernatant was collected to obtain soluble EPS (S-EPS). For loosely bound EPS (LB-EPS), a NaCl solution (0.05%) was added to the residual solid phase before it was washed twice with ultra-pure water. And the volume of solution was adjusted to 40 mL with ultra-pure water. The suspension was subjected to ultrasonication (20 kHz) for 20 min, oscillation (150 rpm) for 10 min, and ultrasonication (20 Hz) for 2 min. The suspension was then centrifuged at 5000*g* for 10 min to achieve solid–liquid separation, and the supernatant was collected to obtain LB-EPS. For tightly bound EPS (TB-EPS), the LB-EPS was washed and resuspended using ultra-pure water before transferring to a water bath at 60 °C for 30 min. After treatment, the samples were centrifuged at 5000*g* for 10 min and the supernatant was collected to obtain TB-EPS. The three EPS extracts were passed through a 0.45 μm PTFE membrane filter to remove large particulate matter prior to 3-D fluorescence excitation emission matrix (EEM) spectroscopy.

Fluorescence EEM spectra were obtained using excitation and emission wavelengths of 200–500 nm (5 nm increments) and 250–600 nm (2 nm increments), respectively, on an F4600 spectrophotometer (Hitachi, Japan). Spectra were recorded at 2400 nm min^{-1} using excitation and emission slot bandwidths of 5 nm and a PMT voltage of 850 V. The EPS content was determined in samples from the fluorescence intensity of the 3D-EEM spectra when their dissolved organic carbon (DOC) content was <10 mg L^{-1}.[30] DOC was measured with a TOC-LC$_{\mathrm{SH/CPH}}$ total organic carbon analyser (Shimadzu, Japan).

The 3D-EEM spectra can be artificially divided into different regions according to the research purpose and the changes in fluorescent substances quantitatively characterized by calculating the volume percentage of a given region.[31] The spectrum was divided into five regions, namely: tyrosine ($\lambda_{\mathrm{ex/em}}$ = 200–250/280–330); tryptophan ($\lambda_{\mathrm{ex/em}}$ = 200–250/330–380); fulvic acid ($\lambda_{\mathrm{ex/em}}$ = 200–250/380–500); soluble microbial products ($\lambda_{\mathrm{ex/em}}$ = 250–400/280–380); and humic acid ($\lambda_{\mathrm{ex/em}}$ = 250–400/380–500). The normalized volume, total volume, and percentage of fluorescence response in each region could be calculated by the following formulas.

$$\Phi_{\mathrm{i,n}} = \mathrm{MF_i}\Phi_{\mathrm{i}} = \mathrm{MF_i}\sum_{\mathrm{ex}}\sum_{\mathrm{em}} I(\lambda_{\mathrm{ex}}\lambda_{\mathrm{em}})\Delta\lambda_{\mathrm{em}} \quad (1)$$

$$\Phi_{\mathrm{T,n}} = \sum \Phi_{\mathrm{i,n}} \quad (2)$$

$$P_{\mathrm{i,n}} = \Phi_{\mathrm{i,n}}/\Phi_{\mathrm{T,n}} \times 100\% \quad (3)$$

where $\Phi_{\mathrm{i,n}}$ is the integrated standard volume of the fluorescence region; Φ_{i} is the integrated volume of the fluorescence region, au nm^2; λ_{ex} is the excitation wavelength, nm; λ_{em} is the emission wavelength, nm; $I(\lambda_{\mathrm{ex}}\lambda_{\mathrm{em}})$ is the fluorescence corresponding to the excitation and emission wavelength intensity, au; $P_{\mathrm{i,n}}$ is the ratio of the integral standard volume of a certain fluorescent area to the total integral standard volume; $\mathrm{MF_i}$ is the multiplication factor, which is equal to the reciprocal of the ratio of the integral area of a certain fluorescent area to the total fluorescent area.

2.4. HMs analysis and potential risk assessment

The HMs in samples were pre-treated by a digestion method. The detailed operations are as follows: adding 0.10 g dry sample to a mixed acid system ($HNO_3 : HClO_4 : HF = 5 : 3 : 3$, v/v/v), using a graphite digestion apparatus under the conditions of 190 °C for 4 h. After using 0.22 μm membrane filters to separate and dilute to an appropriate multiple, the concentrations of Cr, Cu, As, Cd and Pb were determined by inductively coupled plasma mass spectrometry (ICP-MS, Agilent Technologies, 7500CX, Santa, Clara, CA).

The speciation distributions of HMs (Cr, Cu, As, Cd, Pb) in samples were analysed by the three-step extraction procedure from the European Community Bureau of

Reference (BCR),[32] which classified the HMs into four fractions: the exchangeable fraction (F1), reducible fraction (F2), oxidizable fraction (F3), and residual fraction (F4). The details of the BCR sequential extraction procedure were reported by Xie *et al.*[33] All extracts and digestion solutions were filtered through 0.22 μm water-based filter membranes and diluted to a constant volume, and washed twice with ultra-pure water after each fraction was extracted. Finally, the F1, F2, F3 and F4 fractions were determined by ICP-MS.

The leaching toxicity of HMs was analyzed by adopting the TCLP method developed by the United States Environmental Protection Agency (USEPA). TCLP leachates of samples were extracted with a glacial acetic acid solution (sample to acetic acid ratio of 1 : 20) and shaken for 18 h at 200 rpm. The liquid phase was subsequently separated by centrifugation and filtered through 0.22 μm membrane filters before the extracted solutions of HMs were tested with ICP-MS.[34]

The HM potential risk index is used to evaluate the potential pollution risk of solid waste, and its calculation method is as follows.[35]

$$C_\mathrm{f} = W_\mathrm{s}/W_\mathrm{n} \tag{4}$$

$$E_\mathrm{r} = T_\mathrm{f} \cdot C_\mathrm{f} \tag{5}$$

$$\mathrm{RI} = \sum E_\mathrm{r} \tag{6}$$

where W_s is the concentration of F1 + F2 + F3; W_n is the concentration of F4; C_f is a single metal pollution coefficient; T_f is a heavy metal biological toxicity response factor for Cr (2), Cu (5), Zn (1), Cd (30), Pb (5) and As (10), respectively; E_r is a single potential ecological risk coefficient; RI is the potential risk factor. The potential risk assessment indicators (RIs) are shown in the ESI.†

3. Results and discussion

3.1. General properties of DRC and DFCs

The basic properties of DRC and DFCs are summarized in Table 1. The ash content of the DFCs increased with increasing FA addition, while the volatile contents showed the opposite trend. The ash content of DRC (53.17%) was lower than that of DFC85 (61.17%) due to its lower inorganic mineral content. The proximate analysis indicated that the volatile matter content of DRC reached 45.25%, while that of DFC85 decreased to 37.17%. The increase in the C content of DFC100 was attributed to enrichment of the solid phase from carbonization, while the decreases in H and N were likely due to the loss of volatile matter, indicating increased dehydration and decarboxylation in the solid phase.[36] The Ca contents of DRC and DFCs were relatively high, both >26%, while the contents of other mineral elements were relatively low, which indicated that the product has the potential to be used as adsorption materials and building materials.

Table 1 Physicochemical properties of DRC and DFCs

	Proximate analysis (wt%)			Ultimate analysis (wt%)					
Sample	Ash	VM	FC	C	H	N	S	H/C	N/C
DRC	53.17	45.25	1.58	17.57	2.43	2.37	1.19	0.14	0.13
DFC100	57.19	41.77	1.04	20.48	2.31	2.32	1.47	0.11	0.11
DFC95	57.93	40.45	1.62	19.59	2.30	2.49	1.78	0.12	0.13
DFC90	59.41	38.70	1.89	16.89	1.88	1.95	1.78	0.11	0.12
DFC85	61.17	37.17	1.65	15.43	1.84	1.85	2.09	0.12	0.12

	Na	Mg	Al	Si	P	Cl	K	Ca
DRC	0.43	1.34	0.68	1.02	2.07	0.78	0.23	26.10
DFC100	0.42	1.06	0.91	1.28	2.25	0.71	0.23	28.78
DFC95	0.45	1.11	0.79	1.58	1.79	2.54	0.36	31.06
DFC90	0.54	0.95	0.75	1.62	1.48	3.87	0.49	27.98
DFC85	0.56	1.14	0.78	1.80	1.31	5.28	0.66	30.00

3.2. Effects of FA addition on the hydrothermal dehydration of DRs

3.2.1 NCST and solids content. CST and centrifugal solids contents were used to evaluate the dehydration performance of DRs and DFs (Fig. 2). The dehydration performance of DRs was so poor that it cannot be detected for the measurement of CST. Compared with that for DRs, the NCST for DF100 (2.993 s L g^{-1}) decreased rapidly with the addition of 5 wt% FA (0.544 s L g^{-1}), decreasing gradually thereafter. Hence, HTT had a significant effect on the dehydration of DRs, and the addition of FA further improved the performance. The solids content of DRs after centrifugation (19.84 wt%) indicated their poor dehydration performance, which was probably due to the presence of large amounts of bound water.[19] Neyens reported that a temperature ≥175 °C was optimum for the destruction of cellular tissues necessary to improve the dehydration performance of undigested and digested sludges,[37] which can explain the differences in the dehydration effect before and after HTT. Compared with that of DRs, the solids contents of all DFs showed increases ranging from 54.85–102.64% for increasing additions of FA over 5–15 wt% (Fig. 2(b)). These results suggested that moderate additions of FA promoted the dehydration of DRs during the HTT process.

3.2.2 Particle size distribution, zeta potential and viscosity. The particle size distribution can reflect the internal floc structure of DRs. Fig. 3(a) shows the particle size distributions for the suspended solids of DRs and DFs. The $d_{0.5}$ of DRs decreased from 83.49 μm to 35.54 μm after HTT, which can be attributed to the disintegration of large solid particles during HTT. Interestingly, the addition of 5 wt% FA resulted in two peaks of almost equal height in the particle distribution. With further additions of FA, the peak maximum corresponding to the smaller particle diameters gradually increased while other peaks decreased. It is generally accepted that the initial increase in particle size was mainly due to the bridging effect of Ca^{2+} and Maillard reactions.[38] This promoted the agglomeration of small particles into larger particles, thus facilitating flocculation and sedimentation. However, excess FA can result in particle

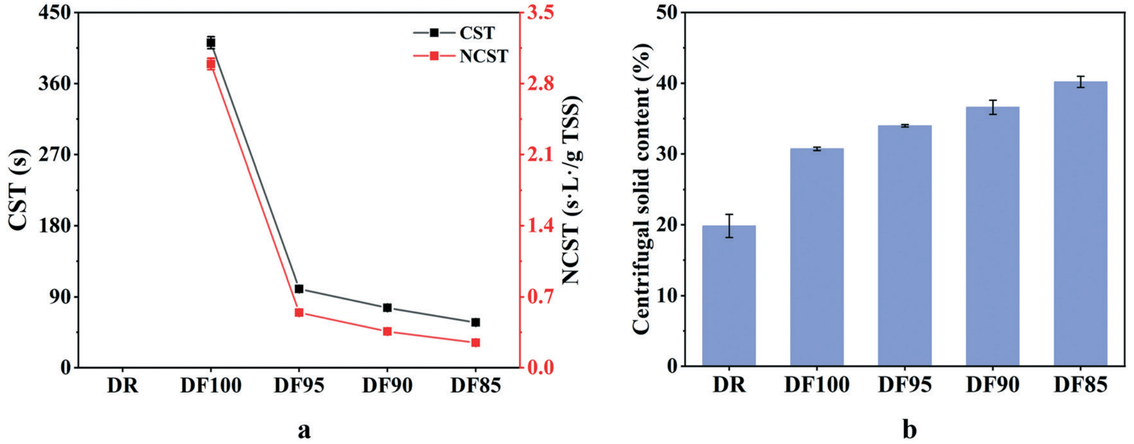

Fig. 2 The effects of FA addition on the NCST and solids contents of DRs and DFs: (a) CST/NCST; (b) centrifugal solids contents.

size reduction, which weakened the bridging and Maillard effects. Therefore, to ensure optimum DR dehydration, a 10 wt% addition of FA was considered appropriate.

According to DLVO (Derjaguin, Landau, Verwey, and Overbeek) theory, the zeta potential is related to the stability of colloidal dispersions which affects DR dehydration performance (the closer to zero potential, the easier it is to flocculate).[39] The evolution of surface charge based on zeta potential measurements is shown in Fig. 3(b). The DRs were negatively charged (zeta potential = −16.60 mV) at room temperature, which was representative of DR flocs, the ionization of protein functional groups in EPS, and other negatively charged substances. After HTT, the zeta potential of DRs showed a significant decrease (−37.4 mV). This indicated that HTT damaged the original structure of DRs, including the rupture of cells and degradation of EPS, leading to the exposure of negatively charged substances within. Following increasing additions of FA, the zeta potential increased from −37.4 to −21.2 mV. The reason for this phenomenon can be attributed to the neutralization of Ca^{2+} in FA. This also indicated that the FA destabilized the HTT residue phase, which was beneficial to the flocculation sedimentation of DRs.

Viscosity is also closely related to the dehydration performance of DRs. As shown in Fig. 3(c), the viscosity of the DRs was high (12 646.7 mPa s), which reflected their poor dehydration performance. After HTT at 180 °C for 30 min, the viscosity of DRs reduced significantly (43.8 mPa s). Under the same conditions, the addition of 5 wt% FA increased the viscosity to 179.9 mPa s, and this decreased with further additions of FA at 10 wt% (121.7 mPa s) and 15 wt% (81.9 mPa s). The viscosity of FAH was 36.1 mPa s. This large change in viscosity after HTT can be attributed to the decomposition of viscous substances in EPS during HTT.[7] The low viscosity of the DFs probably resulted from the outflow of internal bound water in the DRs as a result of the improved dehydration performance of FA. Although the viscosity of DRs increased after adding 5 wt% FA (DF95), it was still relatively low. This phenomenon was due to the promotion of the agglomeration and flocculation of small particles by FA which increased the overall shear force. As the additions of FA increased, the viscosity gradually tended to that of FA. This was also consistent with the measured particle size distributions, *i.e.*, there was a specific FA addition ratio for optimum DR dehydration performance.

3.2.3 EPS analysis. Fig. 4 shows the five regional classifications of S-EPS in DRs and DFs obtained using fluorescence EEM spectroscopy (LB-EPS and TB-EPS are shown in the ESI†). It is generally accepted that higher S-EPS and LB-EPS contents result in poor settleability and

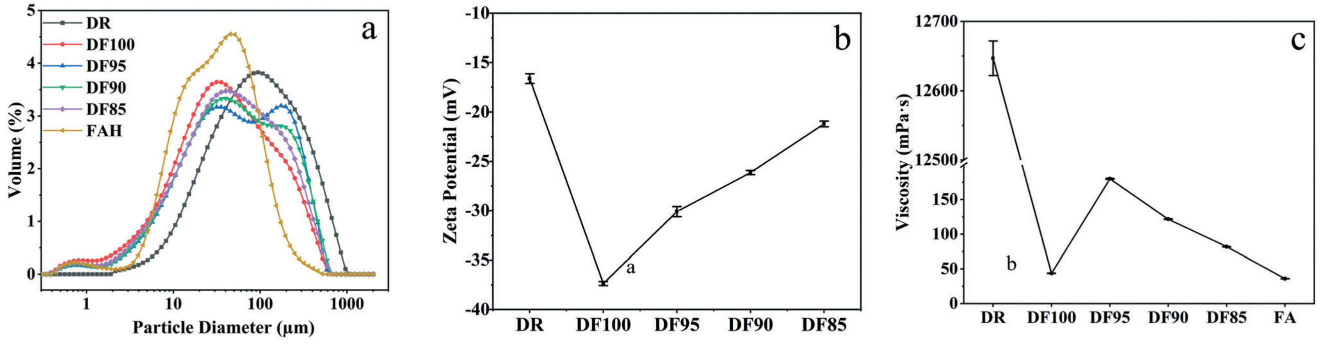

Fig. 3 Particle size distributions, zeta potential and viscosity for DRs and DFs.

dehydration performance due to the weakening of the bonds between cells where protein components play a key role.[40] TB-EPS, on the other hand, is mainly composed of protein-like substances which have greater stability.[41] Three distinct peaks, peak B (EX/EM = 220, 308), peak C (EX/EM = 230, 460), and peak D (EX/EM = 280, 362), and two less distinct peaks, peak A (EX/EM = 225, 308) and peak E (EX/EM = 315, 396), were observed in the EEM spectrum of S-EPS from DF100. As the DRs originated from the same source, there was no obvious shift in peak positions, but some changes in intensity were noted.[42] Peaks A–E denoted the presence of tyrosine, tryptophan, fulvic acids, soluble microbial metabolites, and humic acids, respectively. The fluorescence intensity of DF100 was higher than that of DRs, but this decreased in DF95 and with the further additions of FA. This result indicated that HTT increased biopolymer solubilization by deprotonation of anionic functional groups. In addition, FA can remove protein-like substances, humic acid, and fulvic acid *via* charge neutralization and complexation adsorption, which resulted in decreasing fluorescence intensity. Since DR filtration depends mainly on S-EPS, removal of sticky S-EPS *via* FA addition (conditioning) improved the dehydration performance of DRs.

The composition of EPS is also an important factor affecting dehydration, in which proteins play a more important role than polysaccharides and humic acids.[43] The $P_{\mathrm{i,n}}$ distribution of DRs and DFs (Fig. 5) shows that the proportion of proteins in DRs was 75.94%, which limited their dehydration performance. After HTT, the proportion of proteins decreased sharply (58.78%) due to their denaturation under the hydrothermal conditions. At 10 wt% FA addition, the proportion of proteins increased slightly (64.10%), decreasing to 61.01% at 15 wt% FA. This indicated that the proteins in LB-EPS and TB-EPS may have been converted to S-EPS by FA addition. This was also consistent with the trend in particle size distribution results and indicated that the optimum addition ratio of FA was 10 wt%.

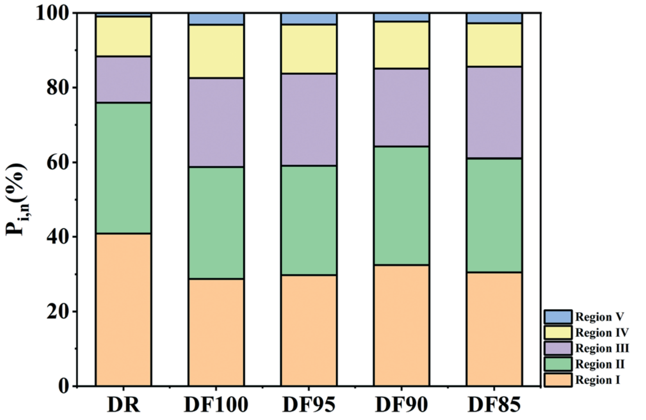

Fig. 5 Fluorescence region integral standard volume composition of DRs and DFs.

3.3. Synergistic hydrothermal dehydration mechanism of DRs and FA

3.3.1 FTIR and SEM analysis. The characteristic peaks of DRC and DFCs determined by FTIR spectroscopy are shown in the ESI.† Peaks characteristic of proteins, polysaccharides, and humus were observed in the spectra of all samples. The following peaks and their assignments were recorded: 1652–1654 cm^{-1}, stretching vibrations of C═O and C–N amide I of the proteins; 1033–1037 cm^{-1}, typical stretching vibration of C–OH and C–O–C in sugar derivatives,[44] a characteristic

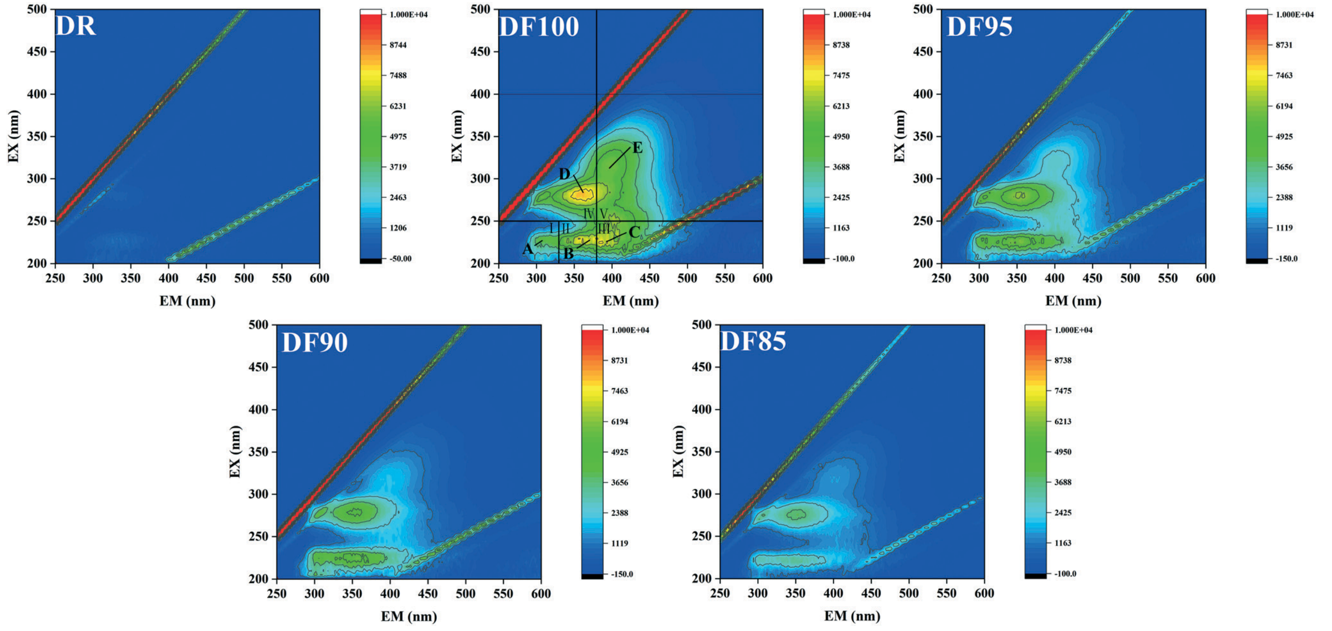

Fig. 4 EEM analysis of S-EPS showing the fluorescence of DRs and DFs.

absorption region of EPS polysaccharides; 2924–2925 cm^{-1} and 1652–1654 cm^{-1}, typical stretching vibrations of C═C related to humic acids; 1445–1455 cm^{-1},[45] deformation of the CH_3 and CH_2 groups of amide III; 3307–3392 cm^{-1}, stretching vibrations of OH and NH_2; 1652–1654 cm^{-1}, characteristic stretching vibration of COOH. The FT-IR results confirmed the presence of EPS components (*e.g.*, polysaccharides, proteins, and humus) in DRs.

The microstructures of DRC and DFCs are shown in the ESI.† The surface of DRs had a relatively dense structure with a few obvious cracks and pore structures, which resulted in a very poor dehydration effect. After HTT, the surface structure of DFC100 showed more small cracks and pores. This was more obvious with increasing additions of FA as the small particles agglomerated into larger units, which agreed with the results of particle size distribution analysis. The results implied that FA can aggravate the destruction of the internal structure of DRs during the hydrothermal process and promote the agglomeration of small particles. This condition was conducive to the formation of a hydrothermal filter cake with a loose structure and well-developed pores.

3.3.2 Dehydration mechanism. Based on the results obtained from the particle size distribution, zeta potential, viscosity, EPS and FTIR analysis, the optimal addition ratio of FA was 10 wt%, and a synergistic hydrothermal dehydration mechanism of DRs and FA was suggested as shown in Fig. 6.

FA addition can increase the zeta potential of DRs after HTT, thereby promoting their instability and benefiting subsequent sedimentation.[46] Calcium ions from the added FA can neutralize the negatively charged components within DRs, including the DR flocs and ionized protein functional groups. In addition, the alkaline environment provided by FA was conducive to cell rupture, and the bridging effects of calcium ions and Maillard reactions can promote flocculation and sedimentation.[38] During HTT, EPS in the DFs was decomposed into smaller molecular substances at the high temperature and pressures involved. These substances, such as polypeptides, fatty acids, glycerol, and monosaccharides, were verified by FTIR. The addition of FA can promote the conversion of TB-EPS and LB-EPS to S-EPS, and the removal of sticky S-EPS *via* FA conditioning could improve the dehydration performance of the treated DRs.[47] Bound water (*i.e.* within cells and between EPS) and interstitial water (*i.e.*, contained in the interstitial space between the DR flocs), which cannot flow freely on the surface of solid DR particles due to surface tension effects,[17] were transformed into free water.

3.4. HM analysis and ecological risk assessment

3.4.1 HM concentrations. The total concentrations of HMs in DRC and DFCs are listed in the ESI.† The HM concentrations in DRC followed the order Cr > Cu > Pb > As > Cd. Generally, the distribution of HMs in DRC was closely related to their source and treatment method, and all HMs were enriched after HTT. Cr, Cu, Cd, and Pb accounted for the majority of HMs in FA and FAH. In contrast, the DRs with low HM toxicity fully exerted a dilution effect in the synergistic hydrothermal treatment of DRs and FA, so that the concentration of HMs in filter cakes was reduced after treatment.

3.4.2 Migration and transformation of HMs. The results obtained from the BCR three-step sequential extraction applied to DRC and DFCs are shown in Fig. 7. F4 accounted for the major proportion of HMs in the materials. For Cr, relatively high proportions were found in the F4 (81.40%) and F3 (17.34%) fractions of DRC. Following HTT, the concentration of Cr in F4 increased (94.09%), while that in F3 decreased (4.73%). The F4 fractions of DFC95 (93.67%), DFC90 (92.40%) and also DFC85 (87.18%) accounted for the largest proportions of Cr. While the relative proportion of Cd decreased with increasing FA addition in F4, the opposite

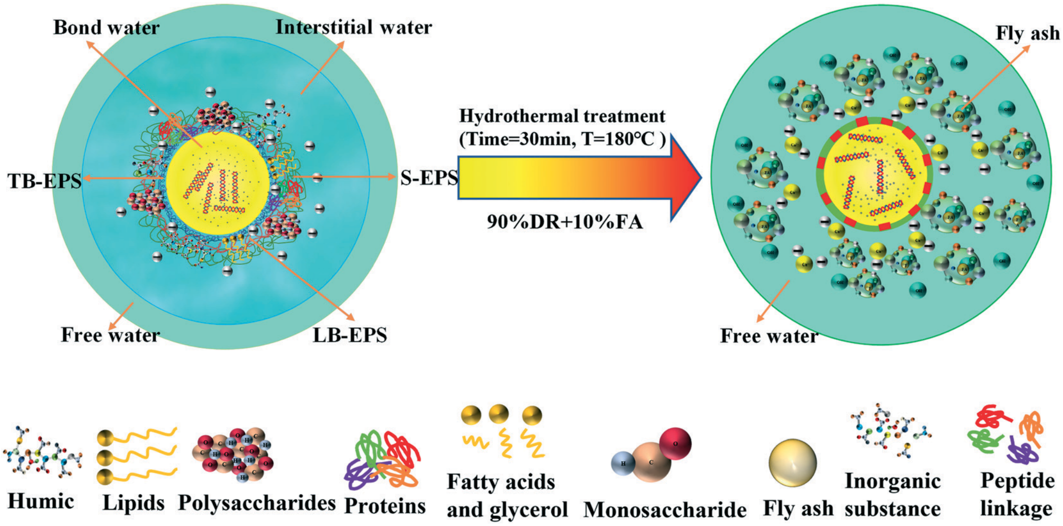

Fig. 6 Synergistic hydrothermal dehydration mechanism of DRs and FA.

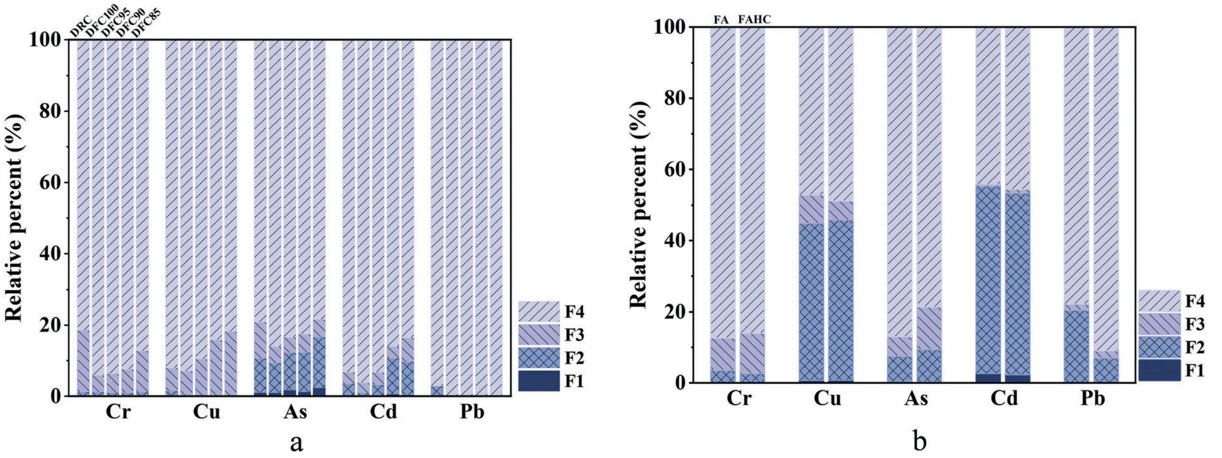

Fig. 7 The distribution of HMs in DRC, DFCs, FA and FAHC: (a) DRs and DFCs; (b) FA and FAHC.

trend was observed for that in F3. For Cu, the F4 fraction of DRC (92.02%) showed little change after HTT (DFC100, 92.93%), decreasing gradually thereafter in DFC95 (89.54%), DFC90 (84.17%), and DFC85 (81.78%). For As, the F4 fractions of DRC (79.12%) increased after HTT (DFC100, 86.02%) and decreased thereafter in DFC95 (83.38%), DFC90 (82.52%), and DFC85 (78.41%). For Cd, the F4 fraction in DRs (93.18%) increased after HTT (DFC100, 96.21%) and decreased thereafter in DFC95 (83.56%), DFC90 (93.24%), and DFC85 (85.98%). The amounts of Pb in F4 ranged from 97.07% (DRC) to 99% (DFCs). The results showed that the increase in the F4 fraction of HMs after DR hydrothermal treatment was due to the complexation and precipitation reactions, where the unstable and loosely adsorbed fractions can be stabilized and re-combined into an organic mineral matrix, during the HTT process.[48,49] In combination with Fig. 7(b), the subsequent addition of fly ash led to a greater dilution than synergistic effect in the change of HM fractions. However, in all hydrothermal samples, the stable F4 fractions were still dominant.

3.4.3 Ecological risk assessment. The TCLP results for DRC and DFCs are shown in Table 2. The leaching concentrations of Cr, Cu, As, Cd, and Pb in all samples were below the standards set by the United States Environmental Protection Agency (USEPA), indicating that the hydrothermal filter cakes can be further utilized without risk to the environment. Note that the leaching concentrations of HMs from DRs and FA were already far below the USEPA threshold values. Hence, HM leaching concentrations were further reduced due to their solidification after HTT.[35]

The ecological risk assessment results are shown in Table 3. The contamination factors (C_f) for Cr, Cu, As, Cd and Pb in DRC (0.030–0.228) were all <1, indicating that the samples were free from contamination. The ecological risk factors (E_r) for the individual elements from DRC and DFCs showed that the materials can meet the requirements of low ecological risk. However, the E_r value for Cd in FA (38.14) was close to the critical value of low ecological risk due to its large proportion in the F2 fraction (51.13%), but the total concentration of Cd was low. The RI index for DRC (5.875) decreased to 3.323 after HTT (DFC100). At FA addition ratios of <15 wt%, the RI indices were <10, demonstrating that the potential ecological risk from the filter cakes was low.

In summary, FA additions of ≤15 wt% cooperatively stabilized HMs during the HTT of DRs, and the potential ecological risks from the five measured HMs were extremely low. Hence, DFCs can be disposed of or further utilized without risk to the environment.[50]

Table 2 Leaching concentrations of HMs from DRs, DFCs, FA and FAHC determined by TLCP

	Leaching concentrations of HMs (mg L^{-1})				
Sample	Cr	Cu	As	Cd	Pb
DRC	0.007 ± 0.002	0.011 ± 0.001	0.053 ± 0.007	0.001 ± 0.000	0.000 ± 0.000
DFC100	0.046 ± 0.00	0.017 ± 0.001	0.059 ± 0.002	0.000 ± 0.000	0.001 ± 0.000
DFC95	0.046 ± 0.001	0.050 ± 0.002	0.067 ± 0.010	0.008 ± 0.001	0.008 ± 0.000
DFC90	0.044 ± 0.003	0.058 ± 0.004	0.107 ± 0.003	0.020 ± 0.001	0.014 ± 0.001
DFC85	0.041 ± 0.001	0.133 ± 0.005	0.162 ± 0.008	0.047 ± 0.002	0.033 ± 0.006
FA	0.244 ± 0.041	0.496 ± 0.097	0.011 ± 0.003	0.008 ± 0.001	0.790 ± 0.150
FAHC	0.212 ± 0.032	0.024 ± 0.000	0.008 ± 0.001	0.008 ± 0.000	0.490 ± 0.015
Threshold[a]	5	—[b]	5	1	5

[a] Threshold values given by the USEPA. [b] Not listed.

Table 3 Potential ecological risk assessment results (C_f, E_r, and RI) for HMs in DRs, DFCs, FA and FAHC

	C_f					E_r					
Sample	Cr	Cu	As	Cd	Pb	Cr	Cu	As	Cd	Pb	RI
DRC	0.228	0.087	0.264	0.073	0.030	0.457	0.433	2.638	2.196	0.151	5.875
DFC100	0.063	0.076	0.162	0.039	0.002	0.126	0.381	1.625	1.182	0.010	3.323
DFC95	0.068	0.117	0.199	0.073	0.001	0.135	0.584	1.993	2.175	0.007	4.894
DFC90	0.082	0.188	0.212	0.163	0.002	0.164	0.940	2.118	4.891	0.008	8.121
DFC85	0.147	0.223	0.275	0.197	0.003	0.294	1.114	2.754	5.901	0.016	10.08
FA	0.146	1.126	0.151	1.271	0.287	0.292	5.629	1.513	38.14	1.433	47.00
FAHC	0.164	1.053	0.274	1.201	0.101	0.328	5.264	2.744	36.04	0.504	44.88

4. Conclusions

This work studied the effects of FA addition on the dehydration of food waste anaerobic DRs using HTT, and the potential environmental risks of HM contamination from the resulting filter cakes. The addition of FA significantly improved the dehydration performance of DRs by reducing NCST, increasing the zeta potential, and improving the particle size distribution. Added FA also promoted the conversion of LB-EPS and TB-EPS to S-EPS and the removal of sticky S-EPS from DRs to improve dehydration performance. 10 wt% addition of FA gave the optimum cooperative dehydration effect of DRs. Meanwhile, DFC90, in which the potential ecological risks of HMs were extremely low, can be used as environmentally friendly materials, such as construction ceramsites, adsorption materials, *etc.*, which is what we are now doing.

Author contributions

Yu Wang: experimental studies, data analysis, and manuscript drafting. Guangwei Yu: conceptualization, supervision, and manuscript drafting. Jiajia Lin, Ruqing Jiang, Xinhai Xu, and Shengyu Xie: data analysis. Yin Wang: resources and supervision. All the authors reviewed the manuscript.

Conflicts of interest

There are no conflicts to declare.

Acknowledgements

This work was supported by the National Key Research and Development Project (2020YFC1908904, 2019YFE0194000), the Natural Science Foundation of Fujian Province (2019J01135), the Strategic Priority Research Program of the Chinese Academy of Sciences (XDA23020504) and the Science and Technology Program of Xiamen (3502Z20193076).

References

1 M. Liu, A. Ogunmoroti, W. Liu, M. Y. Li, M. Y. Bi, W. Q. Liu and Z. J. Cui, *Sci. Total Environ.*, 2022, **807**, 150751.

2 Y. Y. Li, Y. Y. Jin, A. Borrion and H. L. Li, *Bioresour. Technol.*, 2019, **273**, 654–665.

3 J. Lu and S. Y. Xu, *J. Cleaner Prod.*, 2021, **303**, 127033.

4 M. Berglund and P. Brjesson, *Biomass Bioenergy*, 2006, **30**, 254–266.

5 J. X. Liu, S. M. A. Huang, K. Chen, T. Wang, M. Mei and J. P. Li, *Bioresour. Technol.*, 2020, **302**, 122841.

6 S. A. Opatokun, V. Strezov and T. Kan, *Energy*, 2015, **92**, 349–354.

7 C. X. Li, J. Li, L. J. Pan, X. Y. Zhu, S. Y. Xie, G. W. Yu, Y. Wang, X. F. Pan, G. F. Zhu and I. Angelidaki, *J. Cleaner Prod.*, 2020, **265**, 121852.

8 A. Abhishek Kumar, V. R. S. Cheela, D. A. Idiano, I. Eleni, M. R. Islam, J. Michael, T. R. Miller, P. Keshav, P. Alexej, R. Loganath, Z. Min, Z. Caili and L. Jinhui, *Resources, Environment and Sustainability*, 2021, **3**, 100014.

9 T. T. Wang, S. P. Wang, X. Z. Zhong, Z. Y. Sun, Y. L. Huang, L. Tan, Y. Q. Tang and K. Kida, *J. Cleaner Prod.*, 2017, **166**, 530–536.

10 D. Bolzonella, P. Pavan, S. Mace and F. Cecchi, *Water Sci. Technol.*, 2006, **53**, 23–32.

11 M. K. Manu, D. Y. Li, L. W. Luo, J. Zhao, S. Varjani and J. W. C. Wong, *Bioresour. Technol.*, 2021, **334**, 125032.

12 G. P. Zhang, Q. Shi, Q. N. Li, H. T. Wang, H. Y. Yuan, W. J. Guo and Y. F. Lu, *J. Cleaner Prod.*, 2020, **273**, 122907.

13 X. Feng, J. C. Deng, H. Y. Lei, T. Bai, Q. J. Fan and Z. X. Li, *Bioresour. Technol.*, 2009, **100**, 1074–1081.

14 J. B. Liu, Y. S. Wei, K. Li, J. Tong, Y. W. Wang and R. L. Jia, *Water Res.*, 2016, **90**, 225–234.

15 J. P. Zhu, Y. Z. Peng, X. L. Li, G. Q. Su and S. Y. Wang, *Huagong Xuebao*, 2013, **64**, 4210–4215.

16 H. Liu, J. K. Yang, N. R. Zhu, H. Zhang, Y. Li, S. He, C. Z. Yang and H. Yao, *J. Hazard. Mater.*, 2013, **258–259**, 144–150.

17 B. D. Cao, T. Zhang, W. J. Zhang and D. S. Wang, *Water Res.*, 2021, **189**, 116650.

18 M. Citeau, J. Olivier, A. Mahmoud, J. Vaxelaire, O. Larue and E. Vorobiev, *Water Res.*, 2012, **46**, 4405–4416.

19 C. X. Li, X. D. Wang, A. G. Zhang, G. W. Yu, J. J. Lin and Y. Wang, *Water Res.*, 2017, **117**, 49–57.

20 C. X. Li, G. Y. Zhang, Z. K. Zhang, D. C. Ma, L. J. Wang and G. W. Xu, *Chem. Eng. J.*, 2015, **279**, 530–537.

21 S. Y. Xie, G. W. Yu, C. X. Li, F. You, J. Li, R. Tian, G. Wang and Y. Wang, *Environ. Sci. Pollut. Res.*, 2019, **26**, 16537–16547.

22 C. Zhang, M. S. Shao, H. N. Wu, N. Wang, Q. D. Chen and Q. Y. Xu, *Resour., Conserv. Recycl.*, 2021, **171**, 105639.

23 A. Chatterjee, X. J. Hu and F. L. Y. Lam, *Fuel*, 2019, **239**, 726–736.

24 Y. Xue and X. M. Liu, *Chem. Eng. J.*, 2021, **420**, 130349.

25 J. J. Zhang, S. G. Zhang and B. Liu, *J. Cleaner Prod.*, 2020, **250**, 119507.

26 Y. Q. Jin, X. J. Ma, X. G. Jiang, H. M. Liu, X. D. Li, J. H. Yan and K. F. Cen, *Energy Fuels*, 2013, **27**, 394–400.

27 J. L. Xie, Y. Y. Hu, D. Z. Chen and B. Zhou, *Front. Environ. Sci. Eng. China*, 2010, **4**, 108–115.

28 R. P. Merlo, R. S. Trussell, S. W. Hermanowicz and D. Jenkins, *Water Environ. Res.*, 2007, **79**, 320–328.

29 F. W. Gilcreas, *Am. J. Public Health*, 1966, **56**, 387–388.

30 Q. D. Wang, W. J. Zhang, Z. Y. Yang, Q. Y. Xu, P. Yang and D. S. Wang, *Water Res.*, 2018, **146**, 19–29.

31 W. Chen, P. Westerhoff, J. A. Leenheer and K. Booksh, *Environ. Sci. Technol.*, 2003, **37**, 5701–5710.

32 X. D. Wang, V. W. C. Chang, Z. W. Li, Z. Chen and Y. Wang, *J. Hazard. Mater.*, 2021, **412**, 125200.

33 S. Y. Xie, G. W. Yu, R. Q. Jiang, J. L. Ma, X. F. Shang, G. Wang, Y. Wang, Y. A. Yang and C. X. Li, *Biochar*, 2021, **3**, 135–147.

34 X. L. Shen, J. F. Zeng, D. L. Zhang, F. Wang, Y. J. Li and W. M. Yi, *Sci. Total Environ.*, 2020, **704**, 135283.

35 C. X. Li, S. Y. Xie, F. T. You, D. Q. Zhu, J. Li, X. H. Xu, G. W. Yu, Y. Wang and A. Irini, *Waste Manage.*, 2021, **119**, 152–161.

36 M. Alipour, H. Asadi, C. R. Chen and M. R. Rashti, *Ecol. Eng.*, 2021, **162**, 106173.

37 E. Neyens and J. Baeyens, *J. Hazard. Mater.*, 2003, **98**, 51–67.

38 L. Appels, J. Degreve, B. Van der Bruggen, J. Van Impe and R. Dewil, *Bioresour. Technol.*, 2010, **101**, 5743–5748.

39 B. H. Guan, J. Yu, H. L. Fu, M. H. Guo and X. H. Xu, *Water Res.*, 2012, **46**, 425–432.

40 X. Y. Li and S. F. Yang, *Water Res.*, 2007, **41**, 1022–1030.

41 W. Zhang, S. Peng, P. Xiao, J. He, P. Yang, S. Xu and D. Wang, *RSC Adv.*, 2014, **5**, 1282–1294.

42 G. H. Yu, P. J. He and L. M. Shao, *Water Res.*, 2010, **44**, 797–806.

43 W. J. Zhang, P. Yang, X. Y. Yang, Z. Chen and D. S. Wang, *Bioresour. Technol.*, 2015, **181**, 247–253.

44 M. Sun, W. W. Li, Z. X. Mu, H. L. Wang, H. Q. Yu, Y. Y. Li and H. Harada, *Sep. Purif. Technol.*, 2012, **95**, 216–221.

45 X. L. Chai, S. Takayuki, X. Y. Cao, Q. Guo and Y. C. Zhao, *Chemosphere*, 2007, **69**, 1446–1453.

46 J. Yu, M. H. Guo, X. H. Xu and B. H. Guan, *Water Res.*, 2014, **50**, 10–17.

47 P. Yang, D. D. Li, W. J. Zhang, N. Wang, Z. Y. Yang, D. S. Wang and T. Ma, *Chemosphere*, 2019, **218**, 930–940.

48 S. R. Tong, S. P. Zhang, H. X. Yin, J. X. Wang and M. Z. Chen, *J. Anal. Appl. Pyrolysis*, 2021, **155**, 105074.

49 H. J. Huang and X. Z. Yuan, *Bioresour. Technol.*, 2016, **200**, 991–998.

50 X. M. Liu, Y. B. Zhai, S. H. Li, B. Wang, T. F. Wang, Y. L. Liu, Z. Z. Qiu and C. T. Li, *J. Hazard. Mater.*, 2020, **388**, 122084.